Search for new phenomena using single photon events at Lep1

P. Abreu, W. Adam, T. Adye, E. Agasi, I. Ajinenko, R. Aleksan, G.D. Alekseev, R. Alemany, P.P. Allport, S. Almehed, et al.

EUROPEAN ORGANIZATION FOR NUCLEAR RESEARCH

CERN–PPE/96–03

10 January 1996

Search for New Phenomena Using Single Photon Events in the DELPHI Detector at LEP

DELPHI Collaboration

Abstract

Data are presented on the reaction $e^+e^- \to \gamma$ + no other detected particle at center-of-mass energies, $\sqrt{s}$ = 89.48 GeV, 91.26 GeV and 93.08 GeV. The cross section for this reaction is related directly to the number of light neutrino generations which couple to the Z^0 boson, and to several other phenomena such as excited neutrinos, the production of an invisible 'X' particle, a possible magnetic moment of the tau neutrino, and neutral monojets. Based on the observed number of single photon events, the number of light neutrinos which couple to the Z^0 is measured to be $N_\nu = 3.15 \pm 0.34$. No evidence is found for anomalous production of energetic single photons, and upper limits at the 95% confidence level are determined for excited neutrino production (BR $< 4 - 9 \times 10^{-6}$), production of an invisible 'X' particle ($\sigma < 0.1$ pb), and the magnetic moment of the tau neutrino ($< 5.2 \times 10^{-6} \mu_B$). No event with the topology of a neutral monojet is found, and this corresponds to the limit $\sigma < 0.044/\epsilon$ pb at the 95% confidence level, where ϵ is the unknown overall monojet detection efficiency.

(To be submitted to Zeitschr. für Phys. C)

P.Abreu[21], W.Adam[50], T.Adye[37], E.Agasi[31], I.Ajinenko[42], R.Aleksan[39], G.D.Alekseev[16], R.Alemany[49], P.P.Allport[22], S.Almehed[24], U.Amaldi[9], S.Amato[47], A.Andreazza[28], M.L.Andrieux[14], P.Antilogus[9], W-D.Apel[17], Y.Arnoud[39], B.Åsman[44], J-E.Augustin[19], A.Augustinus[9], P.Baillon[9], P.Bambade[19], F.Barao[21], R.Barate[14], M.Barbi[47], G.Barbiellini[46], D.Y.Bardin[16], A.Baroncelli[40], O.Barring[24], J.A.Barrio[26], W.Bartl[50], M.J.Bates[37], M.Battaglia[15], M.Baubillier[23], J.Baudot[39], K-H.Becks[52], M.Begalli[6], P.Beilliere[8], Yu.Belokopytov[9,53], K.Beloous[42], A.C.Benvenuti[5], M.Berggren[47], D.Bertrand[2], F.Bianchi[45], M.Bigi[45], M.S.Bilenky[16], P.Billoir[23], D.Bloch[10], M.Blume[52], S.Blyth[35], T.Bolognese[39], M.Bonesini[28], W.Bonivento[28], P.S.L.Booth[22], G.Borisov[42], C.Bosio[40], S.Bosworth[35], O.Botner[48], E.Boudinov[31], B.Bouquet[19], C.Bourdarios[9], T.J.V.Bowcock[22], M.Bozzo[13], P.Branchini[40], K.D.Brand[36], T.Brenke[52], R.A.Brenner[15], C.Bricman[2], L.Brillault[23], R.C.A.Brown[9], P.Bruckman[18], J-M.Brunet[8], L.Bugge[33], T.Buran[33], T.Burgsmueller[52], P.Buschmann[52], A.Buys[9], S.Cabrera[49], M.Caccia[28], M.Calvi[28], A.J.Camacho Rozas[41], T.Camporesi[9], V.Canale[38], M.Canepa[13], K.Cankocak[44], F.Cao[2], F.Carena[9], L.Carroll[22], C.Caso[13], M.V.Castillo Gimenez[49], A.Cattai[9], F.R.Cavallo[5], L.Cerrito[38], V.Chabaud[9], Ph.Charpentier[9], L.Chaussard[25], J.Chauveau[23], P.Checchia[36], G.A.Chelkov[16], M.Chen[2], R.Chierici[45], P.Chliapnikov[42], P.Chochula[7], V.Chorowicz[9], V.Cindro[43], P.Collins[9], J.L.Contreras[19], R.Contri[13], E.Cortina[49], G.Cosme[19], F.Cossutti[46], H.B.Crawley[1], D.Crennell[37], G.Crosetti[13], J.Cuevas Maestro[34], S.Czellar[15], E.Dahl-Jensen[29], J.Dahm[52], B.Dalmagne[19], M.Dam[29], G.Damgaard[29], P.D.Dauncey[37], M.Davenport[9], W.Da Silva[23], C.Defoix[8], A.Deghorain[2], G.Della Ricca[46], P.Delpierre[27], N.Demaria[35], A.De Angelis[9], W.De Boer[17], S.De Brabandere[2], C.De Clercq[2], C.De La Vaissiere[23], B.De Lotto[46], A.De Min[36], L.De Paula[47], C.De Saint-Jean[39], H.Dijkstra[9], L.Di Ciaccio[38], F.Djama[10], J.Dolbeau[8], M.Donszelmann[9], K.Doroba[51], M.Dracos[10], J.Drees[52], K.-A.Drees[52], M.Dris[32], Y.Dufour[9], D.Edsall[1], R.Ehret[17], G.Eigen[4], T.Ekelof[48], G.Ekspong[44], M.Elsing[52], J-P.Engel[10], N.Ershaidat[23], B.Erzen[43], M.Espirito Santo[21], E.Falk[24], D.Fassouliotis[32], M.Feindt[9], A.Fenyuk[42], A.Ferrer[49], T.A.Filippas[32], A.Firestone[1], P.-A.Fischer[10], H.Foeth[9], E.Fokitis[32], F.Fontanelli[13], F.Formenti[9], B.Franek[37], P.Frenkiel[8], D.C.Fries[17], A.G.Frodesen[4], R.Fruhwirth[50], F.Fulda-Quenzer[19], J.Fuster[49], A.Galloni[22], D.Gamba[45], M.Gandelman[6], C.Garcia[49], J.Garcia[41], C.Gaspar[9], U.Gasparini[36], Ph.Gavillet[9], E.N.Gazis[32], D.Gele[10], J-P.Gerber[10], L.Gerdyukov[42], M.Gibbs[22], R.Gokieli[51], B.Golob[43], G.Gopal[37], L.Gorn[1], M.Gorski[51], Yu.Gouz[45,53], V.Gracco[13], E.Graziani[40], G.Grosdidier[19], K.Grzelak[51], S.Gumenyuk[28,53], P.Gunnarsson[44], M.Gunther[48], J.Guy[37], F.Hahn[9], S.Hahn[52], Z.Hajduk[18], A.Hallgren[48], K.Hamacher[52], W.Hao[31], F.J.Harris[35], V.Hedberg[24], J.J.Hernandez[49], P.Herquet[2], H.Herr[9], T.L.Hessing[35], E.Higon[49], H.J.Hilke[9], T.S.Hill[1], S-O.Holmgren[44], P.J.Holt[35], D.Holthuizen[31], S.Hoorelbeke[2], M.Houlden[22], K.Huet[2], K.Hultqvist[44], J.N.Jackson[22], R.Jacobsson[44], P.Jalocha[18], R.Janik[7], Ch.Jarlskog[24], G.Jarlskog[24], P.Jarry[39], B.Jean-Marie[19], E.K.Johansson[44], L.Jonsson[24], P.Jonsson[24], C.Joram[9], P.Juillot[10], M.Kaiser[17], F.Kapusta[23], K.Karafasoulis[11], M.Karlsson[44], E.Karvelas[11], S.Katsanevas[3], E.C.Katsoufis[32], R.Keranen[4], Yu.Khokhlov[42], B.A.Khomenko[16], N.N.Khovanski[16], B.King[22], N.J.Kjaer[29], H.Klein[9], A.Klovning[4], P.Kluit[31], B.Koene[31], P.Kokkinias[11], M.Koratzinos[9], K.Korcyl[18], C.Kourkoumelis[3], O.Kouznetsov[13,16], P.-H.Kramer[52], M.Krammer[50], C.Kreuter[17], I.Kronkvist[24], Z.Krumstein[16], W.Krupinski[18], P.Kubinec[7], W.Kucewicz[18], K.Kurvinen[15], C.Lacasta[49], I.Laktineh[25], S.Lamblot[23], J.W.Lamsa[1], L.Lanceri[46], D.W.Lane[1], P.Langefeld[52], I.Last[22], J-P.Laugier[39], R.Lauhakangas[15], G.Leder[50], F.Ledroit[14], V.Lefebure[2], C.K.Legan[1], R.Leitner[30], Y.Lemoigne[39], J.Lemonne[2], G.Lenzen[52], V.Lepeltier[19], T.Lesiak[36], D.Liko[50], R.Lindner[52], A.Lipniacka[36], I.Lippi[36], B.Loerstad[24], M.Lokajicek[12], J.G.Loken[35], J.M.Lopez[41], D.Loukas[11], P.Lutz[39], L.Lyons[35], J.MacNaughton[50], G.Maehlum[17], A.Maio[21], V.Malychev[16], F.Mandl[50], J.Marco[41], R.Marco[41], B.Marechal[47], M.Margoni[36], J-C.Marin[9], C.Mariotti[40], A.Markou[11], T.Maron[52], C.Martinez-Rivero[41], F.Martinez-Vidal[49], S.Marti i Garcia[49], F.Matorras[41], C.Matteuzzi[9], G.Matthiae[38], M.Mazzucato[36], M.Mc Cubbin[9], R.Mc Kay[1], R.Mc Nulty[22], J.Medbo[48], M.Merk[31], C.Meroni[28], S.Meyer[17], W.T.Meyer[1], M.Michelotto[36], E.Migliore[45], L.Mirabito[25], W.A.Mitaroff[50], U.Mjoernmark[24], T.Moa[44], R.Moeller[29], K.Moenig[9], M.R.Monge[13], P.Morettini[13], H.Mueller[17], L.M.Mundim[6], W.J.Murray[37], B.Muryn[18], G.Myatt[35], F.Naraghi[14], F.L.Navarria[5], S.Navas[49], K.Nawrocki[51], P.Negri[28], S.Nemecek[12], W.Neumann[52], N.Neumeister[50], R.Nicolaidou[3], B.S.Nielsen[29], M.Nieuwenhuizen[31], V.Nikolaenko[10], P.Niss[44], A.Nomerotski[36], A.Normand[35], W.Oberschulte-Beckmann[17], V.Obraztsov[42], A.G.Olshevski[16], A.Onofre[21], R.Orava[15], K.Osterberg[15], A.Ouraou[39], P.Paganini[19], M.Paganoni[9], P.Pages[10], H.Palka[18], Th.D.Papadopoulou[32], K.Papageorgiou[11], L.Pape[9], C.Parkes[35], F.Parodi[13], A.Passeri[40], M.Pegoraro[36], L.Peralta[21], H.Pernegger[50], M.Pernicka[50], A.Perrotta[5], C.Petridou[46], A.Petrolini[13], M.Petrovyck[28,53], H.T.Phillips[37], G.Piana[13], F.Pierre[39], M.Pimenta[21], M.Pindo[28], S.Plaszczynski[19], O.Podobrin[17], M.E.Pol[6], G.Polok[18], P.Poropat[46], V.Pozdniakov[16], M.Prest[46], P.Privitera[38], N.Pukhaeva[16], A.Pullia[28], D.Radojicic[35], S.Ragazzi[28], H.Rahmani[32], J.Rames[12], P.N.Ratoff[20], A.L.Read[33], M.Reale[52], P.Rebecchi[19], N.G.Redaelli[28], M.Regler[50], D.Reid[9], P.B.Renton[35], L.K.Resvanis[3], F.Richard[19], J.Richardson[22], J.Ridky[12], G.Rinaudo[45], I.Ripp[39], A.Romero[45], I.Roncagliolo[13], P.Ronchese[36], L.Roos[14], E.I.Rosenberg[1], E.Rosso[9], P.Roudeau[19], T.Rovelli[5], W.Ruckstuhl[31], V.Ruhlmann-Kleider[39], A.Ruiz[41], K.Rybicki[18], H.Saarikko[15], Y.Sacquin[39], A.Sadovsky[16], G.Sajot[14], J.Salt[49], J.Sanchez[26], M.Sannino[13], M.Schimmelpfennig[17], H.Schneider[17], U.Schwickerath[17], M.A.E.Schyns[52], G.Sciolla[45], F.Scuri[46], P.Seager[20], Y.Sedykh[16], A.M.Segar[35], A.Seitz[17], R.Sekulin[37], R.C.Shellard[6], I.Siccama[31], P.Siegrist[39], S.Simonetti[39], F.Simonetto[36], A.N.Sisakian[16], B.Sitar[7], T.B.Skaali[33], G.Smadja[25], N.Smirnov[42], O.Smirnova[16], G.R.Smith[37], O.Solovianov[42], R.Sosnowski[51], D.Souza-Santos[6], T.Spassov[21], E.Spiriti[40], P.Sponholz[52], S.Squarcia[13], C.Stanescu[40], S.Stapnes[33], I.Stavitski[36], F.Stichelbaut[9], A.Stocchi[19], J.Strauss[50], R.Strub[10], B.Stugu[4], M.Szczekowski[51], M.Szeptycka[51], T.Tabarelli[28],

J.P.Tavernet[23], O.Tchikilev[42], A.Tilquin[27], J.Timmermans[31], L.G.Tkatchev[16], T.Todorov[10], D.Z.Toet[31], A.Tomaradze[2], B.Tome[21], A.Tonazzo[28], L.Tortora[40], G.Transtromer[24], D.Treille[9], W.Trischuk[9], G.Tristram[8], A.Trombini[19], C.Troncon[28], A.Tsirou[9], M-L.Turluer[39], I.A.Tyapkin[16], M.Tyndel[37], S.Tzamarias[22], B.Ueberschaer[52], O.Ullaland[9], V.Uvarov[42], G.Valenti[5], E.Vallazza[9], C.Vander Velde[2], G.W.Van Apeldoorn[31], P.Van Dam[31], W.K.Van Doninck[2], J.Van Eldik[31], N.Vassilopoulos[35], G.Vegni[28], L.Ventura[36], W.Venus[37], F.Verbeure[2], M.Verlato[36], L.S.Vertogradov[16], D.Vilanova[39], P.Vincent[25], L.Vitale[46], E.Vlasov[42], A.S.Vodopyanov[16], V.Vrba[12], H.Wahlen[52], C.Walck[44], M.Weierstall[52], P.Weilhammer[9], C.Weiser[17], A.M.Wetherell[9], D.Wicke[52], J.H.Wickens[2], M.Wielers[17], G.R.Wilkinson[35], W.S.C.Williams[35], M.Winter[10], M.Witek[18], K.Woschnagg[48], K.Yip[35], O.Yushchenko[42], F.Zach[25], A.Zaitsev[42], A.Zalewska[18], P.Zalewski[51], D.Zavrtanik[43], E.Zevgolatakos[11], N.I.Zimin[16], M.Zito[39], D.Zontar[43], R.Zuberi[35], G.C.Zucchelli[44], G.Zumerle[36]

[1] Ames Laboratory and Department of Physics, Iowa State University, Ames IA 50011, USA
[2] Physics Department, Univ. Instelling Antwerpen, Universiteitsplein 1, B-2610 Wilrijk, Belgium
and IIHE, ULB-VUB, Pleinlaan 2, B-1050 Brussels, Belgium
and Faculté des Sciences, Univ. de l'Etat Mons, Av. Maistriau 19, B-7000 Mons, Belgium
[3] Physics Laboratory, University of Athens, Solonos Str. 104, GR-10680 Athens, Greece
[4] Department of Physics, University of Bergen, Allégaten 55, N-5007 Bergen, Norway
[5] Dipartimento di Fisica, Università di Bologna and INFN, Via Irnerio 46, I-40126 Bologna, Italy
[6] Centro Brasileiro de Pesquisas Físicas, rua Xavier Sigaud 150, RJ-22290 Rio de Janeiro, Brazil
and Depto. de Física, Pont. Univ. Católica, C.P. 38071 RJ-22453 Rio de Janeiro, Brazil
and Inst. de Física, Univ. Estadual do Rio de Janeiro, rua São Francisco Xavier 524, Rio de Janeiro, Brazil
[7] Comenius University, Faculty of Mathematics and Physics, Mlynska Dolina, SK-84215 Bratislava, Slovakia
[8] Collège de France, Lab. de Physique Corpusculaire, IN2P3-CNRS, F-75231 Paris Cedex 05, France
[9] CERN, CH-1211 Geneva 23, Switzerland
[10] Centre de Recherche Nucléaire, IN2P3 - CNRS/ULP - BP20, F-67037 Strasbourg Cedex, France
[11] Institute of Nuclear Physics, N.C.S.R. Demokritos, P.O. Box 60228, GR-15310 Athens, Greece
[12] FZU, Inst. of Physics of the C.A.S. High Energy Physics Division, Na Slovance 2, 180 40, Praha 8, Czech Republic
[13] Dipartimento di Fisica, Università di Genova and INFN, Via Dodecaneso 33, I-16146 Genova, Italy
[14] Institut des Sciences Nucléaires, IN2P3-CNRS, Université de Grenoble 1, F-38026 Grenoble Cedex, France
[15] Research Institute for High Energy Physics, SEFT, P.O. Box 9, FIN-00014 Helsinki, Finland
[16] Joint Institute for Nuclear Research, Dubna, Head Post Office, P.O. Box 79, 101 000 Moscow, Russian Federation
[17] Institut für Experimentelle Kernphysik, Universität Karlsruhe, Postfach 6980, D-76128 Karlsruhe, Germany
[18] Institute of Nuclear Physics and University of Mining and Metalurgy, Ul. Kawiory 26a, PL-30055 Krakow, Poland
[19] Université de Paris-Sud, Lab. de l'Accélérateur Linéaire, IN2P3-CNRS, Bât. 200, F-91405 Orsay Cedex, France
[20] School of Physics and Materials, University of Lancaster, Lancaster LA1 4YB, UK
[21] LIP, IST, FCUL - Av. Elias Garcia, 14-1^{o}, P-1000 Lisboa Codex, Portugal
[22] Department of Physics, University of Liverpool, P.O. Box 147, Liverpool L69 3BX, UK
[23] LPNHE, IN2P3-CNRS, Universités Paris VI et VII, Tour 33 (RdC), 4 place Jussieu, F-75252 Paris Cedex 05, France
[24] Department of Physics, University of Lund, Sölvegatan 14, S-22363 Lund, Sweden
[25] Université Claude Bernard de Lyon, IPNL, IN2P3-CNRS, F-69622 Villeurbanne Cedex, France
[26] Universidad Complutense, Avda. Complutense s/n, E-28040 Madrid, Spain
[27] Univ. d'Aix - Marseille II - CPP, IN2P3-CNRS, F-13288 Marseille Cedex 09, France
[28] Dipartimento di Fisica, Università di Milano and INFN, Via Celoria 16, I-20133 Milan, Italy
[29] Niels Bohr Institute, Blegdamsvej 17, DK-2100 Copenhagen 0, Denmark
[30] NC, Nuclear Centre of MFF, Charles University, Areal MFF, V Holesovickach 2, 180 00, Praha 8, Czech Republic
[31] NIKHEF-H, Postbus 41882, NL-1009 DB Amsterdam, The Netherlands
[32] National Technical University, Physics Department, Zografou Campus, GR-15773 Athens, Greece
[33] Physics Department, University of Oslo, Blindern, N-1000 Oslo 3, Norway
[34] Dpto. Fisica, Univ. Oviedo, C/P. Pérez Casas, S/N-33006 Oviedo, Spain
[35] Department of Physics, University of Oxford, Keble Road, Oxford OX1 3RH, UK
[36] Dipartimento di Fisica, Università di Padova and INFN, Via Marzolo 8, I-35131 Padua, Italy
[37] Rutherford Appleton Laboratory, Chilton, Didcot OX11 OQX, UK
[38] Dipartimento di Fisica, Università di Roma II and INFN, Tor Vergata, I-00173 Rome, Italy
[39] Centre d'Etudes de Saclay, DSM/DAPNIA, F-91191 Gif-sur-Yvette Cedex, France
[40] Istituto Superiore di Sanità, Ist. Naz. di Fisica Nucl. (INFN), Viale Regina Elena 299, I-00161 Rome, Italy
[41] Instituto de Fisica de Cantabria (CSIC-UC), Avda. los Castros, S/N-39006 Santander, Spain, (CICYT-AEN93-0832)
[42] Inst. for High Energy Physics, Serpukov P.O. Box 35, Protvino, (Moscow Region), Russian Federation
[43] J. Stefan Institute and Department of Physics, University of Ljubljana, Jamova 39, SI-61000 Ljubljana, Slovenia
[44] Fysikum, Stockholm University, Box 6730, S-113 85 Stockholm, Sweden
[45] Dipartimento di Fisica Sperimentale, Università di Torino and INFN, Via P. Giuria 1, I-10125 Turin, Italy
[46] Dipartimento di Fisica, Università di Trieste and INFN, Via A. Valerio 2, I-34127 Trieste, Italy
and Istituto di Fisica, Università di Udine, I-33100 Udine, Italy
[47] Univ. Federal do Rio de Janeiro, C.P. 68528 Cidade Univ., Ilha do Fundão BR-21945-970 Rio de Janeiro, Brazil
[48] Department of Radiation Sciences, University of Uppsala, P.O. Box 535, S-751 21 Uppsala, Sweden
[49] IFIC, Valencia-CSIC, and D.F.A.M.N., U. de Valencia, Avda. Dr. Moliner 50, E-46100 Burjassot (Valencia), Spain
[50] Institut für Hochenergiephysik, Österr. Akad. d. Wissensch., Nikolsdorfergasse 18, A-1050 Vienna, Austria
[51] Inst. Nuclear Studies and University of Warsaw, Ul. Hoza 69, PL-00681 Warsaw, Poland
[52] Fachbereich Physik, University of Wuppertal, Postfach 100 127, D-42097 Wuppertal 1, Germany
[53] On leave of absence from IHEP Serpukhov

1 Introduction

Annihilation events in e^+e^-collisions which feature no charged particles in the final state are used to estimate the number of light neutrino generations which couple to the Z^0 via the reaction $e^+e^- \to \nu\bar{\nu}\gamma$. They may also provide a clear signal for new phenomena such as the existence of excited neutrinos [1]. In addition, they allow limits to be set on a possible magnetic moment for the tau neutrino [2] and on the production of an invisible 'X' particle in association with a photon. Also, the selection criteria used for the analysis allow the search for events having the characteristics of neutral monojets, which would be neutral jets which contain some electromagnetic energy and which are detected as several distinct neutral showers.

The essence of this analysis is to measure the cross section for the reaction $e^+e^- \to \gamma$ + no other detected particle using the DELPHI detector [3] at the CERN LEP collider.

In section 2, aspects of the DELPHI detector pertinent to this analysis are presented. In section 3, the data sample and event selection criteria are presented. A discussion of the uncertainties and backgrounds is given in section 4, and in section 5 results on the number of light neutrino generations are presented. Results on searches for new physics, including excited neutrinos, the tau neutrino magnetic moment, an invisible 'X' particle, and neutral monojets are presented in section 6. Lastly, the conclusions are given.

2 The DELPHI Detector

The search for single photon events in the DELPHI detector [3,4] depends largely on the features of the barrel electromagnetic calorimeter, the High-density Projection Chamber (HPC) [5]. The rest of the DELPHI detector is used specifically to veto on the presence of any other particles in the final state and to measure the integrated luminosity.

The HPC is a gas sampling calorimeter which uses a long drift time to provide complete three-dimensional charge information in the manner of a time-projection chamber. It subtends the angular range $41° < \vartheta < 139°$, where ϑ is the polar angle to the beam direction, and it is mounted directly inside the 5.2-meter (inner diameter) superconducting solenoid of DELPHI, which provides a 1.23 Tesla axial magnetic field. The HPC consists of 144 modules arranged in 24 azimuthal sectors, where each sector consists of six modules along the beam axis.

Each module consists of 41 layers of lead radiator totalling about 18 radiation lengths (X_0) at normal incidence, interspersed with 40 gas sampling slots containing a mixture of argon and methane gases. Charge due to ionization produced in the electromagnetic showers drifts along the beam (z) axis in parallel electric and magnetic fields, and is read out via a grid of 128 cathode pads per module, which provides nine samplings along the shower axis. The 15 MHz sampling frequency corresponds to a cell size of 3.5 mm along the beam axis, with a spatial resolution varying between 1.3 and 3.1 mm according to the polar angle. The granularity in the azimuthal angle (ϕ) is about 20 mrad.

The HPC electromagnetic calorimeter is described in the literature [5] as is the readout electronics [6]. The energy resolution of the HPC is determined from a study of the Bhabha events (45 GeV electromagnetic showers) plus a study of π^0 reconstructed in the calorimeter. The energy resolution of the HPC is $\sigma/\mathrm{E} = 0.043 \oplus 0.32/\sqrt{\mathrm{E}}$, where the symbol $\oplus$ means addition in quadrature, and E is in GeV [4]. The quoted resolution includes the effects of about 0.7 X_0 of material in front of the HPC.

The DELPHI single photon trigger uses a positive correlation between a signal from the HPC first-level trigger which comes from a layer of plastic scintillator inserted in each

module near shower maximum, and a signal from the HPC second-level trigger which uses a pattern of charge in the module itself. The scintillator provides a fast (< 2 μsec) first-level trigger from each module. To provide a second-level trigger, signals from the cathode pads which represent electric charge accumulated in the module from a shower are split. They are sent to the FADC's for digitization, and they also provide input to the second level trigger. For the second level trigger, the signals from the 18432 HPC cathode pads are added in groups of 16 to provide 8 signals per module (1152 for the entire HPC).

To keep the background levels low, the correlation between the first and second level triggers is performed on groups of three adjacent HPC modules at the same azimuth. For details see reference [7].

The trigger efficiency is determined in an analysis using about 8000 Compton scatter events in which the scattered electron (or positron) enters an HPC module, and the photon is detected in a forward electromagnetic calorimeter (see below). The positron (or electron) escapes undetected down the beam pipe. These events are particularly clean, and they provide a sample of known electromagnetic showers in the HPC in which the incident energy is known both from the kinematics of Compton scattering and also from measurement of the electron curvature. The trigger efficiency is shown in Figure 1. This measurement is an update of an earlier measurement by the same method which used the 1993 data [7]. The systematic uncertainty in the measured cross sections due to the trigger efficiency, determined from the fit shown in Figure 1, averages to 13% over the observed single photon energy spectrum. It is included in all cross section uncertainties quoted below.

Measurement of cross sections requires knowledge of the integrated luminosity. The Small Angle Tagger (SAT) [3] was the main luminosity monitor in DELPHI before the 1994 run. It consisted of two cylindrical calorimeters placed ± 232.5 cm from the beam interaction point and covering the polar angular region from 43 mrad to 135 mrad. Each cylinder was composed of a set of circular sheets of lead and scintillating fibres arranged inside an aluminum support. The total depth was equivalent to 20 X_0. On one side a tungsten mask defined with high precision the inner radius of the detector and prevented off-momentum particles from entering the calorimeter through the internal surface.

The read-out segmentation was defined by 3 cm rings in the r coordinate and 7.5° in ϕ for the four outermost rings and 15° for the others. The energy resolution was $\sigma/\mathrm{E} = 0.012 \oplus 0.114/\sqrt{\mathrm{E}} + 0.023$, where E is in GeV [3].

The principal source of background to the reaction $e^+e^- \to \nu\bar{\nu}\gamma$ is the radiative Bhabha reaction $e^+e^- \to e^+e^-\gamma$ in which the final state electron and positron escape detection. This may occur in the 1993 data if the electron and positron emerge at angles below the SAT acceptance ($\vartheta < 43$ mrad) or in the region between the SAT and the forward electromagnetic calorimeter (FEMC), i.e. 135 mrad $< \vartheta <$ 173 mrad. In the 1994 data, the SAT was replaced with a new luminosity monitor, and this is discussed in detail below.

The DELPHI Forward Electromagnetic Calorimeter (FEMC) [4] subtends a polar angle $10° < \vartheta < 37°$ and $143° < \vartheta < 170°$. It consists of two 5 m diameter disks with a total of 9064 lead glass blocks in the form of truncated pyramids arranged to point just 3° from the interaction point. The lead glass counters (20 X_0 deep, 5 x 5 cm^2, $\sim$1° x 1°) are read out with vacuum photodiodes. The energy resolution is $\sigma/\mathrm{E} = 0.03 \oplus 0.12/\sqrt{\mathrm{E}} \oplus 0.11/\mathrm{E}$, with E in GeV, the last term being due to amplification noise. At LEP the energy resolution is degraded by about two radiation lengths of material in front of the calorimeter. Electron showers at 45 GeV from Bhabha scatter events are measured with $\sigma/\mathrm{E} = 4.8\%$.

For the 1994 run, a new luminosity monitor, the Small Angle TIle Calorimeter (STIC) was installed in the DELPHI detector [4]. It consists of two identical calorimeters with radial and azimuthal segmentation located at $\pm$220 cm from the interaction point, with an angular coverage between 29 and 185 mrad. Each STIC detector is a lead-scintillator sampling calorimeter (49 layers of 3.4 mm steel laminated lead plates and 3 mm thick scintillator for a total of $\sim$ 27 X_0) with wavelength shifter fiber readout, and is equipped with two planes of silicon strip detectors placed after 4 and 7.4 radiation lengths. The geometry of each calorimeter is projective with respect to the interaction point, and the lower radial acceptance is defined with high precision (20 μm) by a tungsten mask placed in front of one of the calorimeters. The uncertainty in the measured luminosity is less than one per mill. Test beam measurements give an energy resolution of $\sigma/\mathrm{E} = 0.0152 \oplus 0.135/\sqrt{\mathrm{E}}$, with E in GeV. At 45.6 GeV the measured energy resolution is σ/E =2.7% [4].

The DELPHI tracking system is divided into a number of independent devices which include the vertex detector (VD), inner detector (ID), time projection chamber (TPC), and outer detector (OD) in the barrel region, plus forward chambers A and B which enhance tracking close to the beam direction. The effective range of charged particle tracking is $11° < \vartheta < 169°$. Detailed descriptions of these detectors are found in reference [4]

3 Data Sample and Event Selection

This analysis is based on data collected with the DELPHI detector [3,4] at the CERN LEP collider during the second half of the 1993 run and throughout 1994. The start date is necessitated by the absence of a true single photon trigger in DELPHI before then.

In a scan of the Z^0 peak during the 1993 run, data were recorded at three center-of-mass energies, $\sqrt{s}$ = 89.48 GeV, 91.26 GeV, and 93.08 GeV. The 1994 run was entirely at $\sqrt{s}$ = 91.2 GeV. The integrated luminosities during the period in which the DELPHI single photon trigger was operational in 1993 and 1994 were determined by measuring Bhabha scattering at very small angles using the small angle tagger (SAT) calorimeter for the 1993 run, and the scintillating tile calorimeter (STIC) luminosity monitor for the 1994 run. The integrated luminosities for those runs in which both the TPC and HPC were fully operational are shown in Table 1.

For this analysis, single photon events are used where the photon has been detected in the HPC electromagnetic calorimeter.

The data sample is defined by the following requirements:

(a) The most energetic neutral particle in the barrel be measured in the HPC;
(b) $\mathrm{E}_\gamma > 2$ GeV, where E_γ is the measured energy of the shower in the HPC; and
(c) $|\cos\vartheta_\gamma| < 0.7$, where ϑ_γ is the polar angle of the photon with respect to the beam axis.

Cuts (a), (b) and (c) define the kinematic region of interest. For photon energies below 2 GeV or photon polar angles to the beam axis below 45°, radiative Bhabha background (see section 4) dominates the $\nu\bar{\nu}\gamma$ signal.

(d) The shower must contain energy clusters in at least three of the nine pad layers of the HPC module;
(e) the first energy cluster of the shower must be in one of the first three pad layers of the HPC module; and

(f) no one pad layer of the HPC may contain more than 90% of the total shower energy.

Cuts (d), (e) and (f) are used to ensure a clean electromagnetic shower in the HPC and to discriminate against alpha decays from radioactive inclusions in the HPC lead converter.

(g) There should be no significant evidence of any other neutral particle in the event, i.e. a second neutral would veto the event if (i) it were an HPC shower with E > 0.5 GeV, it passed cuts (d) and (f) above, and it were more than 20° from the candidate photon, or (ii) it were not an HPC shower with E > 2 GeV, and it were more than 20° from the candidate photon. Such non-HPC neutrals are detected in the hadron calorimeter, forward electromagnetic calorimeter, or luminosity monitors (SAT or STIC).

Cut (g) reduces two-gamma and three-gamma events to a negligible level. The 20° algorithm is used, rather than a blanket veto by any second neutral because the HPC pattern recognition occasionally produces small satellite showers close to an energetic primary neutral shower. Also, it allows the possibility of the search for neutral monojets.

A total of 2215 events survive the above cuts. All these events were scanned by physicists to verify the presence of a single electromagnetic shower in the HPC electromagnetic calorimeter and the absence of evidence for any other particles in the event. Most of the rejected events were showers caused by cosmic rays or residual alpha decays. Although the pattern of individual hits in several detectors made cosmic ray events relatively easy to detect visually, the occasional failure of any of these hits to produce an accepted charged track segment made it difficult to eliminate all cosmic ray events by computer before the scan. A similar situation was true for the events caused by alpha decays. Results of the scan are shown in Table 2. After the scan two additional cuts are imposed:

(h) The azimuthal and polar angles of the shower axis, as determined in a fit to the spatial distribution of the individual charge clusters in the HPC, must each be within 15° of the azimuthal and polar angles of the line from the vertex to the shower charge barycenter. Figure 2 shows the differences in polar and azimuthal angles between the shower axis and the line to the shower barycenter, separately for events identified in the scan as single photons and those labelled cosmic ray events.

(i) To be accepted the event had to be triggered by the single photon trigger described earlier. (Some events also satisfied other DELPHI triggers, some of which use the HPC and which have some single photon capability.) The trigger cut was imposed late in the analysis to allow an investigation of this trigger's efficiency for different types of events.

The final sample of single photon events passing all the cuts described above is 219 events.

Figure 3 shows the distributions in the photon energy, E_γ, for the single photon events. The histograms show the predictions of the theoretical calculations for $\nu\bar{\nu}\gamma$ and $e^+e^-\gamma$ events as described below. The calculated distributions include all cuts and efficiencies. The double peak structure in the background distribution ($e^+e^-\gamma$) corresponds to final state electrons and positrons which escape detection either by going down the beam pipe or into the region between the SAT and the FEMC for the 1993 data only. As mentioned above, for the 1994 data there is no gap between the STIC and the FEMC.

4 Uncertainties and Backgrounds

Apart from the integrated luminosity discussed earlier and the statistical uncertainty in the number of events observed, measurement of a cross section requires knowledge of the trigger and reconstruction efficiencies. The trigger efficiency has been discussed in section 2.

The efficiency for detecting photons in the accepted region of the HPC, i.e. $E_\gamma > 2$ GeV and $|\cos\vartheta_\gamma| < 0.7$, is less than unity because (i) even within this region there are dead spaces between HPC modules, and thus there is some probability that a photon may enter a dead region and fail to be detected, and (ii) the criteria for labelling a signal in the HPC as a legitimate electromagnetic shower are less than 100% efficient even for photons of energy greater than 2 GeV. Specifically, this arises because statistical fluctuations in the deposited charge in a single pad row are occasionally large enough to cause no recorded signal above threshold in that row. For low energy showers, the loss of signal in a single row may sometimes cause the entire shower to fail the criteria for a legitimate electromagnetic shower. In addition, a significant fraction of photons convert in the material of the detector before the HPC. Those photons that convert in front of the TPC produce charged tracks. Those that convert closer to the HPC, e.g. in the outer detector [4], are often still reconstructed as single neutral showers in the HPC.

The photon detection and reconstruction efficiency is calculated by generating large numbers of single photon events according to phase space, i.e. uniform in $\cos\vartheta$ and in azimuthal angle. These events are passed through the standard DELPHI detector simulation and event reconstruction codes. The efficiency is estimated as the fraction which pass the single photon selection criteria. Systematic errors arise because of edge effects near the boundaries of the HPC modules and to the finite energy resolution of the calorimeter. For $E_\gamma > 2$ GeV, the single photon detection and reconstruction efficiency is computed to be 0.67 ± 0.01, and it is approximately independent of photon energy [8]. This includes all effects described above, except for the single photon trigger efficiency.

It is also necessary to consider the possibility of a charged particle, e.g. an electron, arriving at the HPC undetected by all the inner detectors and producing an electromagnetic shower, which would then be mislabelled as a photon. Monte Carlo calculations indicate that this contribution would be less than 0.1 events, which may be neglected.

There are three possibly significant backgrounds to true single photon events. They are (i) radiative Bhabha scatters in which the final state electron and positron escape detection, typically by going down the beam pipe or into a crack in the detector, (ii) $e^+e^- \to \gamma\gamma$ events in which the second photon escapes detection, and (iii) $e^+e^- \to \gamma\gamma\gamma$ events in which two of the photons escape detection.

The cross section for radiative Bhabha scattering, i.e. the reaction $e^+e^- \to e^+e^-\gamma$, in which the photon satisfies the cuts and both the outgoing electron and positron escape detection, is difficult to calculate in general. It involves detailed Monte Carlo generation of radiative Bhabha scatters including radiative corrections [9], and it also involves detailed simulation of the apparatus to include properly all the effects related to whether or not the outgoing electron or positron is detected and thus can veto the event. For neutrino counting, these problems are compounded by the fact that the cross section for radiative Bhabha scattering is a priori much greater than that for $\nu\bar{\nu}\gamma$. However, radiative Bhabha scattering results in a photon angular distribution more strongly peaked in the forward-backward direction than that for $\nu\bar{\nu}\gamma$. The fraction of radiative Bhabha scatters with a photon produced at an angle to the beam direction, $\vartheta_\gamma > \vartheta_{min}$, is

$$f(\vartheta_{min}) \approx \frac{m_e^2}{\vartheta_{min}^2 \cdot \mathrm{E}_{beam}^2} \tag{1}$$

The strict energy and angle cuts on the photon ($\mathrm{E}_\gamma > 2$ GeV and $\mid \cos\vartheta_\gamma \mid < 0.7$), together with the rejection of events with reconstructed charged tracks or high energy deposition in the forward calorimeters, reduces the background from radiative Bhabha scatters to a low level (see next section and Table 3).

Results of two calculations of the radiative Bhabha background (Mana & Martinez and TEEGG. See ref. [9]), with the photon satisfying all appropriate cuts and the final state electron and positron both escaping detection, are in good agreement to within less than 1%.

The cross sections for the reactions $e^+e^- \to \gamma\gamma(\gamma)$ are large. Specifically, the cross section for electron-positron annihilation into two photons is given by:

$$\frac{d\sigma}{dy}(e^+e^- \to \gamma\gamma) = \frac{2\pi\alpha^2}{s} \cdot \frac{1+y^2}{1-y^2} \tag{2}$$

where $y = \cos\vartheta_\gamma$. For this reaction, the two photons must both be energetic ($\mathrm{E}_\gamma = \sqrt{s}/2$), and they must be emitted in opposite directions. The probability of exactly one of them escaping detection is very small, and thus this background to true single photon events is relatively small (see next section and Table 3).

Since the process $e^+e^- \to \gamma\gamma\gamma$ is the same as the two-photon reaction with the third photon the product of initial state radiation, one of the three photons is generally forward and of relatively low energy so it may easily escape detection. The other two photons need not be back-to-back in this case, and therefore the probability of losing one of them in a crack and detecting the other is larger than in the two-γ case. Cut (g) described in section 3 removes most of the two-γ and three-γ events. Monte Carlo calculations [9], including the same cuts and efficiencies as for the data, compute the sum of the two-γ and three-γ cross sections. The result is a prediction of 4.1 events expected, with nine events observed in the scan. The contamination from $e^+e^- \to \gamma\gamma(\gamma)$ events in the sample labelled single γ events is negligible.

Other possible backgrounds include $e^+e^- \to \mu^+\mu^-\gamma$ and $e^+e^- \to \tau^+\tau^-\gamma$, which have been measured (see reference [10]), and $e^+e^- \to \gamma\pi^0$, $e^+e^- \to \gamma\mathrm{n}\bar{\mathrm{n}}$, and $e^+e^- \to \gamma\pi^0\pi^0$, for which there are theoretical expectations [10]. These have all been calculated and found to be negligible in the accepted kinematic region. In addition, a calculation of potential backgrounds from resonances which are produced in two-photon interactions and decay into several π^0's, only one photon from which is detected, shows that this effect is negligible with the severe cuts imposed.

5 Results on the Number of Light Neutrino Generations

In the reaction $e^+e^- \to \nu\bar{\nu}\gamma$, the photon is the result of initial state radiation by either the electron or the positron, and the $\nu\bar{\nu}$ pair is produced either by the decay of a Z^0 boson produced in the s-channel or by W-exchange in the t-channel. In addition, the s-channel and t-channel amplitudes interfere. The suggestion to use this reaction to determine the number of light neutrino generations which couple to the Z^0 has been made many times [11–16].

The number of light neutrino generations, N_ν, may be calculated from the cross section for the reaction $e^+e^- \to \nu\bar{\nu}\gamma$ in a specific kinematic region since the dependence of the doubly differential cross section on N_ν is known. It is given in reference [13] as

$$\frac{d^2\sigma}{dxdy} = \frac{G_F^2 \alpha s(1-x)[(1-x/2)^2 + x^2y^2/4]}{6\pi^2 x(1-y^2)} \times$$

$$\left(2 + \frac{N_\nu(g_V^2+g_A^2) + 2(g_V+g_A)[1-s(1-x)/M_Z^2]}{[1-s(1-x)/M_Z^2]^2 + \Gamma_Z^2/M_Z^2}\right) \qquad (3)$$

neglecting radiative corrections (discussed below).

In equation (3) G_F is the Fermi coupling constant, α is the fine structure constant, s is the square of the center-of-mass energy, x is the photon energy in units of the incident beam energy, y is the cosine of the photon's momentum angle with respect to the incident beam direction, i.e. $y = \cos\vartheta_\gamma$, N_ν is the number of low-mass neutrino generations, M_Z is the mass of the Z^0 , and Γ_Z is the total width of the Z^0. For M_Z and Γ_Z the averages of measurements by the four LEP experiments, as quoted in reference [17], are used, i.e., $M_Z = 91.1888 \pm 0.0044$ GeV and $\Gamma_Z = 2.4974 \pm 0.0038$ GeV. In the standard model of Glashow, Weinberg, and Salam [18], $g_V = -\frac{1}{2} + 2\sin^2\vartheta_W$ and $g_A = -\frac{1}{2}$, where ϑ_W is the weak mixing angle. It is worth noting that in equation (3) the $(g_V^2 + g_A^2)$ term is from the square of the s-channel Z^0 amplitude, the "2" term is from the square of the t-channel W-exchange amplitude, and the $(g_V + g_A)$ term is from $Z^0 - W$ interference.

Thus, the cross section for $e^+e^- \to \nu\bar{\nu}\gamma$ may be calculated if the analytic formula is integrated over the appropriate kinematic region. The integration may be performed either numerically or by generating $\nu\bar{\nu}\gamma$ events by Monte Carlo techniques and recording the fraction which survive the kinematic cuts. In this work, numerical integration over the allowed fiducial region is used to calculate the cross sections, and the generation of events by Monte Carlo techniques is used to determine the efficiencies.

Radiative corrections must also be included. Since in the reaction $e^+e^- \to \nu\bar{\nu}\gamma$, there is no final state radiation (and therefore no interference between initial and final state radiation), the uncertainties about radiative corrections which plague the background reactions, e.g. radiative Bhabha scatters, are much less severe for $\sigma_{\nu\bar{\nu}\gamma}$. The radiative corrections modify equation (3) both in line shape and in cross section [19].

The results of the calculations of $e^+e^- \to \nu\bar{\nu}\gamma$ [19] and $e^+e^- \to e^+e^-\gamma$ [9], and the calculation of the cross section for $e^+e^- \to \nu\bar{\nu}\gamma$, based on the number of observed events, are shown in Table 3.

Figure 4 shows the measured values of the cross section for $e^+e^- \to \nu\bar{\nu}\gamma$ in the accepted region, i.e. $E_\gamma > 2$ GeV and $|\cos\vartheta_\gamma| < 0.7$, at the three center-of-mass energies. In addition, curves which represent the integral of equation (3) over the region of the cuts are plotted. To generate these curves, N_ν is set equal to 2, 3 and 4 generations respectively in the theoretical calculations [19]. A fit of the three data points to the integral of equation (3) with N_ν left as a free parameter yields $N_\nu = 3.15 \pm 0.34$ as the number of light neutrino generations with a χ^2 of 1.5 for two degrees of freedom. This result is consistent with the number of light neutrino generations found by other methods and also by this method in the other LEP collaborations [20].

6 Searches for New Physics

Events featuring a single highly energetic photon can provide evidence for the presence of new physics. In the selected sample, presented in section 3, a total of fifteen true single photon events have $E_\gamma > 10$ GeV, while six of these events have $E_\gamma > 15$ GeV. A total of 8.4 such events are expected with $E_\gamma > 10$ GeV and 2.9 events with $E_\gamma > 15$ GeV from the neutrino counting reaction $e^+e^- \to \nu\bar{\nu}\gamma$ [19], while, the contribution from the radiative Bhabha reaction, in which the final state electron and positron are undetected, is negligible in this region. No event is observed with $E_\gamma > 22$ GeV. Standard Model processes populate the low end of the single photon energy spectrum, and these data show no evidence for an anomalous source of high energy single photons. This result is consistent with the results of the other LEP collaborations [21]. In the following, limits on possible sources of new physics will be determined on the basis of these observations.

6.1 Results on Excited Neutrinos

Excited neutrinos can be produced at LEP either in pairs through the reaction $e^+e^- \to \nu^*\bar{\nu^*}$ or singly through the reaction $e^+e^- \to \nu^*\bar{\nu}$ [1]. The cross section for pair production is independent of the compositeness scale Λ. Present LEP limits already exclude this channel for excited neutrino masses below $\sqrt{s}\ /2$ [22]. The single production of excited neutrinos, which depends on the $Z\nu^*\bar{\nu}$ couplings, allows the lower limit on the branching fraction of the Z^0 into $\nu^*\bar{\nu}$ to be extended to values of M_{ν^*} up to M_Z. With the assumption of a pure left-handed or right-handed ν^*, the cross section for $Z^0 \to \nu^*\bar{\nu}$ is just the $Z^0 \to \nu\bar{\nu}$ cross section [23], apart from kinematical factors,

$$\frac{\sigma_{\nu^*\bar{\nu}}}{\sigma_{\nu\bar{\nu}}} = \frac{s}{\Lambda^2}(1 - \frac{M^2_{\nu^*}}{s})^2(1 + 2\frac{M^2_{\nu^*}}{s}) \tag{4}$$

Events with single ν^* production are generated according to equation (4) for a number of M_{ν^*} values. The branching fraction of ν^* into $\nu\gamma$ is assumed equal to unity, and a (1 + cos α) angular distribution is assumed for the radiative decay of the ν^*, where α is the polar angle of the neutrino momentum in the ν^* rest frame defined with respect to the ν^* momentum direction in the center-of-mass frame. The efficiency depends slightly on the value of M_{ν^*} for the mass region considered, and it varies between 20% and 30%, including the trigger efficiency. The upper limit at the 95% confidence level for BR($Z^0 \to \nu^*\bar{\nu}$) as a function of M_{ν^*} is shown in Figure 5. This limit, expressed in terms of the effective coupling constant λ/M_{ν^*}, is shown in Figure 5, and with the effective coupling defined as [24]

$$\frac{\lambda}{M_{\nu^*}} = \frac{1}{\sqrt{2}\Lambda} \tag{5}$$

The "kink" at about 60 GeV is kinematical in origin. Specifically, for $M_{\nu^*} > 60$ GeV, E_γ may be in the full range from 2 to 45 GeV.

6.2 Results on the Tau Neutrino Magnetic Moment

The magnetic moment coupling of the tau neutrino gives a contribution to the differential cross section for the process $e^+e^- \to \nu\bar{\nu}\gamma$ of the form [2]

$$\frac{d\sigma}{xdxdy} = \frac{\alpha^2\kappa^2}{96\pi}\mu_B^2 C[\chi_w]F[s,x,y] \tag{6}$$

where x is the photon energy in units of the incident beam energy, y is the cosine of the photon polar angle with respect to the beam axis, and κ is the anomalous magnetic moment of the tau neutrino in units of the Bohr magneton, μ_B. The kinematics are contained in the function

$$F[s,x,y] \equiv (\frac{s^2}{4}) \cdot \frac{1-x+x^2(1-y^2)/8}{(s-M_Z^2)^2+M_Z^2\Gamma_Z^2} \tag{7}$$

and the coefficient C is given by

$$C[\chi_w] \equiv \frac{8\chi_w^2-4\chi_w+1}{\chi_w^2(1-\chi_w)^2} \tag{8}$$

with $\chi_w \equiv \sin^2\vartheta_w$ and using the Standard Model $Ze^+e^-$and $Z\nu\bar{\nu}$ couplings. Initial state radiation is neglected in the above formulation. Photon and W exchange graphs contribute about 1% in the kinematic region of interest, and these also have been neglected in equation (6).

If the tau neutrino magnetic moment were $\mu_\nu = 5\times10^{-6}\mu_B$, then 90% of the increase over the Standard Model prediction would be in the energy region above 22 GeV.

After integrating equation (6) over the kinematically allowed region, with $E_\gamma > 22$ GeV and $|\cos\vartheta_\gamma| < 0.7$, the estimated cross section expected due to a neutrino magnetic moment at $\sqrt{s} = M_Z$ is

$$\sigma = 6.6 \text{ mb} \times \kappa^2 \tag{9}$$

Taking into account the other two center-of-mass energy points and correcting for initial state radiation, the null observation of events with $E_\gamma > 22$ GeV yields a limit on an anomalous magnetic moment for ν_τ of

$$\kappa < 5.2\times10^{-6} \tag{10}$$

at the 95% confidence level. A similar measurement has been reported by the L3 collaboration [25]. It is worth noting that since the photons are real this limit is at $Q^2 = 0$. A more stringent limit has been obtained by a different technique using the BEBC bubble chamber [26].

6.3 Search for γ'X' Production

A new particle 'X' may be produced in association with a photon in the reaction $e^+e^- \to \gamma$'X'. If particle 'X' is invisible or can decay invisibly, then it could be seen in the single photon topology. Figure 6(a) shows the distribution in recoil mass against the photon for the 219 single photon events. The distribution is consistent with that expected from known sources. Figure 6(b) shows the upper limit at the 95% confidence level of the cross section for $Z^0 \to \gamma$'X' as a function of the mass of 'X' with the photon produced in the angular region $|\cos\vartheta_\gamma| < 0.7$. The limit is calculated assuming that the width of the 'X' particle (including resolution) is less than the bin width. This limit is similar to that found by the OPAL collaboration [27].

6.4 Search for Neutral Monojets

The selection criteria described in section 3 allow a search for events having a topology of neutral monojets. In fact, events with several neutral showers are not rejected, provided the neutrals are within a cone of 20^0 half angle. Notice also that neutrals reconstructed

in the hadronic calorimeters would not veto such events. No neutral monojet event is observed in the scan. In order to extract a limit on the production cross section, no specific hypothesis is made on the possible origin of such neutral monojets. Therefore, in the absence of a model specifying monojet mass and decay multiplicity, the limit quoted below is given as a function of the unknown overall detection efficiency for neutral monojets. The null observation of such neutral monojets yields a limit on the production cross section in the Z^0 energy range of

$$\sigma < 0.044/\epsilon \text{ pb} \tag{11}$$

at the 95% confidence level, where ϵ is the overall efficiency for their observation. If it is assumed that the energy dependence of the production of neutral monojets follows the Z^0 line shape, and if it is further assumed that the overall efficiency for their observation is for example 10%, then the limit on the Z^0 branching ratio into neutral monojets would be

$$BR(Z^0 \rightarrow \text{neutral monojets}) < 1.2 \times 10^{-5} \tag{12}$$

at the 95% confidence level.

7 Conclusions

Data are presented on the reaction $e^+e^- \rightarrow \gamma$ + no other detected particle at center-of-mass energies, $\sqrt{s}$ = 89.48 GeV, 91.26 GeV and 93.08 GeV. The measured cross section for this reaction is used to determine the number of light neutrino generations which couple to the Z^0 boson. The result is $N_\nu = 3.15 \pm 0.34$. No evidence is found for sources of highly energetic single photons other than the known Standard Model processes, and new upper limits at the 95% confidence level are set on the production of excited neutrinos (see Fig. 5), on the production of an invisible particle 'X' via the reaction $e^+e^- \rightarrow \gamma$'X' (see Fig. 6), and on a possible tau neutrino magnetic moment ($\kappa < 5.2 \times 10^{-6}$ at the 95% confidence level). No event with the topology of a neutral monojet has been found, and this corresponds to a cross section limit of $\sigma < 0.044/\epsilon$ pb at the 95% confidence level, where ϵ is the overall efficiency for observation of neutral monojets.

Acknowledgements

We are greatly indebted to our technical collaborators and to the funding agencies for their support in building and operating the DELPHI detector, and to the members of the CERN-SL Division for the excellent performance of the LEP collider.

References

[1] F. Boudjema and Djouadi, Phys. Lett. **B240** (1990) 485.

[2] Thomas M. Gould and I. Z. Rothstein, Phys. Lett. **B333** (1994) 545.

[3] P. Aarnio, et. al. (DELPHI Collaboration), Nucl. Instr. and Meth. **A303** (1991) 233.

[4] P. Abreu, et al. (DELPHI Collaboration), "Performance of the DELPHI Detector", CERN–PPE/95-194 , submitted to Nucl. Instr. and Meth.

[5] H. G. Fischer, Nucl. Instr. and Meth., **A265** (1988) 218;
F. L. Navarria, et al., Nucl. Instr. and Meth., **A257** (1987) 499;
A. Cattai, et al., Nucl. Instr. and Meth., **A235** (1985) 310;
E. I. Rosenberg, "The DELPHI High Density Projection Chamber", in *Proceedings of the Gas Sampling Calorimetry Workshop II*, Fermilab, Batavia, Il. (1985) 450;
H. G. Fischer and O. Ullaland, IEEE Trans. Nucl. Sci., **NS-27** (1980) 38.

[6] H. B. Crawley, et al., IEEE Trans. Nucl. Sci., **NS-35** (1988) 295;
H. B. Crawley, et al., IEEE Trans. Nucl. Sci., **NS-34** (1987) 261.

[7] D. Gillespie and T. Malmgren, "The First and Second Level HPC Trigger Simulation", DELPHI 94-46 CAL 155, 2 May 1994.

[8] W. Adam, et al., (DELPHI Collaboration), "Measurement of Inclusive π^0 Production in Hadronic Z^0 Decays", CERN–PPE/95-144, submitted to Z. Phys. C.

[9] For the generator of the process $e^+e^- \to \nu\bar{\nu}\gamma$ see F. A. Berends, et al., Nucl. Phys. **B301** (1988) 583, and R. Miquel, C. Mana and M. Martinez, Z. Phys. **C48** (1990) 309.
For radiative corrections see C. Mana and M. Martinez, Nucl. Phys. **B287** (1987) 601, and F. A. Berends, G. J. H. Burgers, C. Mana, M. Martinez, and W. L. van Neerven, CERN-TH 4865/87.
For radiative corrections to the background processes $e^+e^- \to e^+e^-\gamma$, $\gamma\gamma$, or $\gamma\gamma\gamma$ see F. A. Berends, K. J. F. Gaemers and R. Gastmans, Nucl. Phys. **B57** (1973) 381, **B63** (1973) 381, and **B68** (1979) 541; F. A. Berends and R. Kleiss, Nucl. Phys. **B177** (1981) 237 and **B186** (1981) 22; Dean Karlen, Nucl. Phys. **B289** (1987) 23.
For the KORALZ generator see S. Jadach, B. F. L. Ward and Z. Was, Comp. Phys. Comm. **66** (1991) 276.

[10] For $e^+e^- \to \mu^+\mu^-\gamma$ see J. Bartels, et al., Z. Phys. **C23** (1984) 295. For $e^+e^- \to \tau^+\tau^+\gamma$ the contribution to the background with the photon in the region of the cuts and none of the charged particles from the tau decays vetoing the event is even smaller than for $e^+e^- \to \mu^+\mu^-\gamma$. For $e^+e^- \to \gamma\pi^0$, $\gamma n\bar{n}$, and $\gamma\pi^0\pi^0$ see Ernest Ma and Jon Okada, Phys. Rev. Lett. **41** (1978) 287.

[11] Ernest Ma and Jon Okada, op. cit. See previous reference.

[12] K. J. F. Gaemers, R. Gastmans, and F. M. Renard, Phys. Rev. **D19** (1979) 1605.

[13] G. Barbiellini, B. Richter, and J. L. Siegrist, Phys. Lett. **106B** (1981) 414.

[14] J. Bartels, A. Fridman, A. Schwarz, and Tai Tsun Wu, Z. Phys. **C23** (1984) 295.

[15] M. Caffo, R. Gatto, and E. Remiddi, Phys. Lett. **B173** (1986) 91.

[16] Elmar Lieb, "Radiative Neutrinozählung mit dem DELPHI-Detektor auf der Z^0-Resonanz" Diplomarbeit, Bergische Universität - Gesamthochschule Wuppertal, WU D 88 - 30 (1988).

[17] D. Schaile, in "Proceedings of the XXVII International Conference on High Energy Physics", 20-27 July 1994, Glasgow, Scotland, UK, page 27.

[18] S. L. Glashow, Nucl. Phys. **B22** (1961) 579; S. Weinberg, Phys. Rev. Lett. **19**

(1967) 1264; A. Salam, Proceedings of the 8th Nobel Symposium, p. 367, May 1968, Ed. N. Svartholm, New York, Wiley 1968.
[19] O. Nicrosini and L. Trentadue, Phys. Lett. **B196** (1987) 551;
O. Nicrosini and L. Trentadue, Nucl. Phys. **B318** (1989) 1.
[20] D. Buskulic, et al. (ALEPH Collaboration), Phys. Lett. **B313** (1993) 520;
B. Adeva, et al. (L3 Collaboration), Phys. Lett. **B275** (1992) 209;
O. Adriani, et al. (L3 Collaboration), Phys. Lett. **B292** (1992) 463;
M. Z. Akrawy, et al. (OPAL Collaboration), Z. Phys. **C50** (1991) 373;
R. Akers, et al. (OPAL Collaboration), Z. Phys. **C65** (1995) 47.
[21] O. Adriani, et al. (L3 Collaboration), Phys. Lett. **B297** (1993) 469;
R. Akers, et al., op. cit. See previous reference.
[22] D. Decamp, et al. (ALEPH Collaboration), Phys. Lett. **B250** (1990) 172;
P. Abreu, et al. (DELPHI Collaboration), Phys. Lett. **B274** (1992) 230;
D. Bertrand, et al. (DELPHI Collaboration), "Search for an Excited Neutrino Using the DELPHI Detector", DELPHI 92-111 PHYS 217;
B. Adeva, et al. (L3 Collaboration), Phys. Lett. **B252** (1990) 525.
[23] K. Hagiwara, S. Komamiya and Z. Zeppenfeld, Z. Phys. **C29** (1985) 115.
[24] P. Abreu, et al. (DELPHI Collaboration), Z. Phys. **C53** (1992) 41.
[25] M. Acciarri, et al. (L3 Collaboration), Phys. Lett. **B346** (1995) 190. For a direct comparison with this L3 result, the DELPHI limit corresponds to $\kappa < 4.5 \times 10^{-6}$ at the 90% confidence level.
[26] A. M. Cooper-Sarkar, et al., Phys. Lett. **B280** (1992) 153.
[27] R. Akers, et al., op. cit. See reference [20].

$\sqrt{s}$ (GeV)	$\int \mathcal{L}\,\mathrm{dt}$ (pb^{-1})
89.48	7.532 $\pm$ 0.006
91.26	52.462 $\pm$ 0.032
93.08	7.645 $\pm$ 0.008
Total	67.639 $\pm$ 0.034

Table 1: Integrated luminosity at the three center-of-mass energies.

Scan Result	Number of Events	
	All Scanned	All Cuts
Single γ	319	219
Alpha	1222	244
Cosmic	433	45
Noise	216	47
$e^+e^- \to \gamma\gamma(\gamma)$	13	6
$e^+e^- \to e^+e^-$	12	1
Total	2215	562

Table 2: Results of the visual scan.

$\sqrt{s}$ =	89.48 GeV	91.26 GeV	93.08 GeV
Predicted σ (pb) ($N_\nu = 3$)	4.3	9.9	33.0
Calculated N_{events}			
$e^+e^- \to \nu\bar{\nu}\gamma$	11.0 $\pm$ 0.6	126.6 $\pm$ 9.5	50.0 $\pm$ 3.9
$e^+e^- \to e^+e^-\gamma$	8.1 $\pm$ 0.9	19.3 $\pm$ 1.9	7.4 $\pm$ 0.8
$N_{expected}$	19.1 $\pm$ 1.1	145.9 $\pm$ 9.7	57.4 $\pm$ 4.0
$N_{observed}$	21	148	50
$N_{corrected}$	60 $\pm$ 15	519 $\pm$ 79	251 $\pm$ 48
$\sigma(\nu\bar{\nu}\gamma)$ (pb)	7.9 $\pm$ 2.0	9.9 $\pm$ 1.5	32.8 $\pm$ 6.3

Table 3: Numbers of events and cross sections for the reaction $e^+e^- \to \nu\bar{\nu}\gamma$ in the kinematic region $E_\gamma > 2$ GeV and $|\cos\vartheta_\gamma| < 0.7$. The row $N_{corrected}$ contains the corrected number of events after the calculated background ($e^+e^-\gamma$) is subtracted and the corrections for trigger and reconstruction efficiencies are applied.

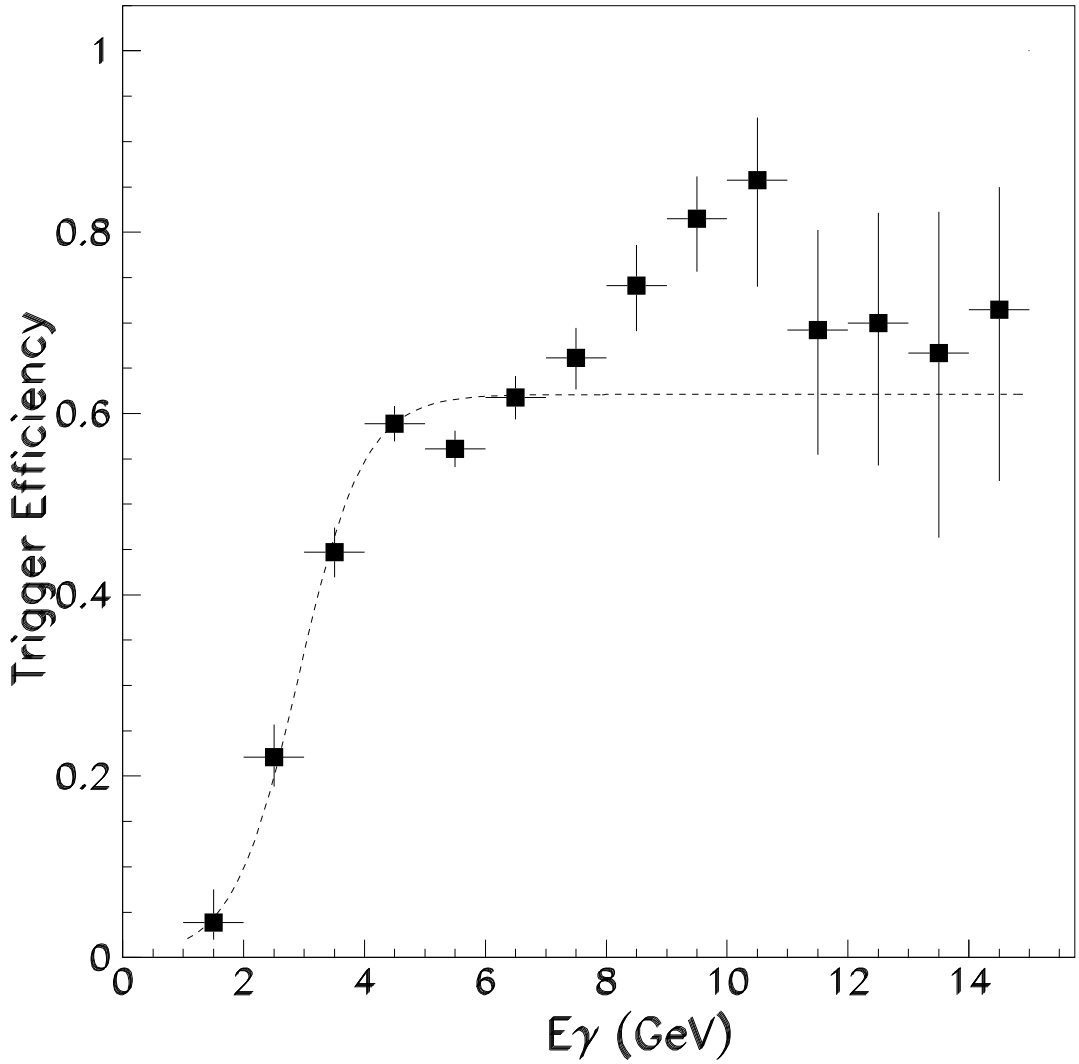

Figure 1: Single photon trigger efficiency in the HPC as determined from Compton scatter events. The curve shows the result of a fit to the function $\epsilon(E_\gamma) = A/(Be^{-E_\gamma * C} + 1)$, with A = 0.64 $\pm$ 0.01, B = 68. $\pm$ 30., and C = 1.41 $\pm$ 0.15 GeV^{-1}.

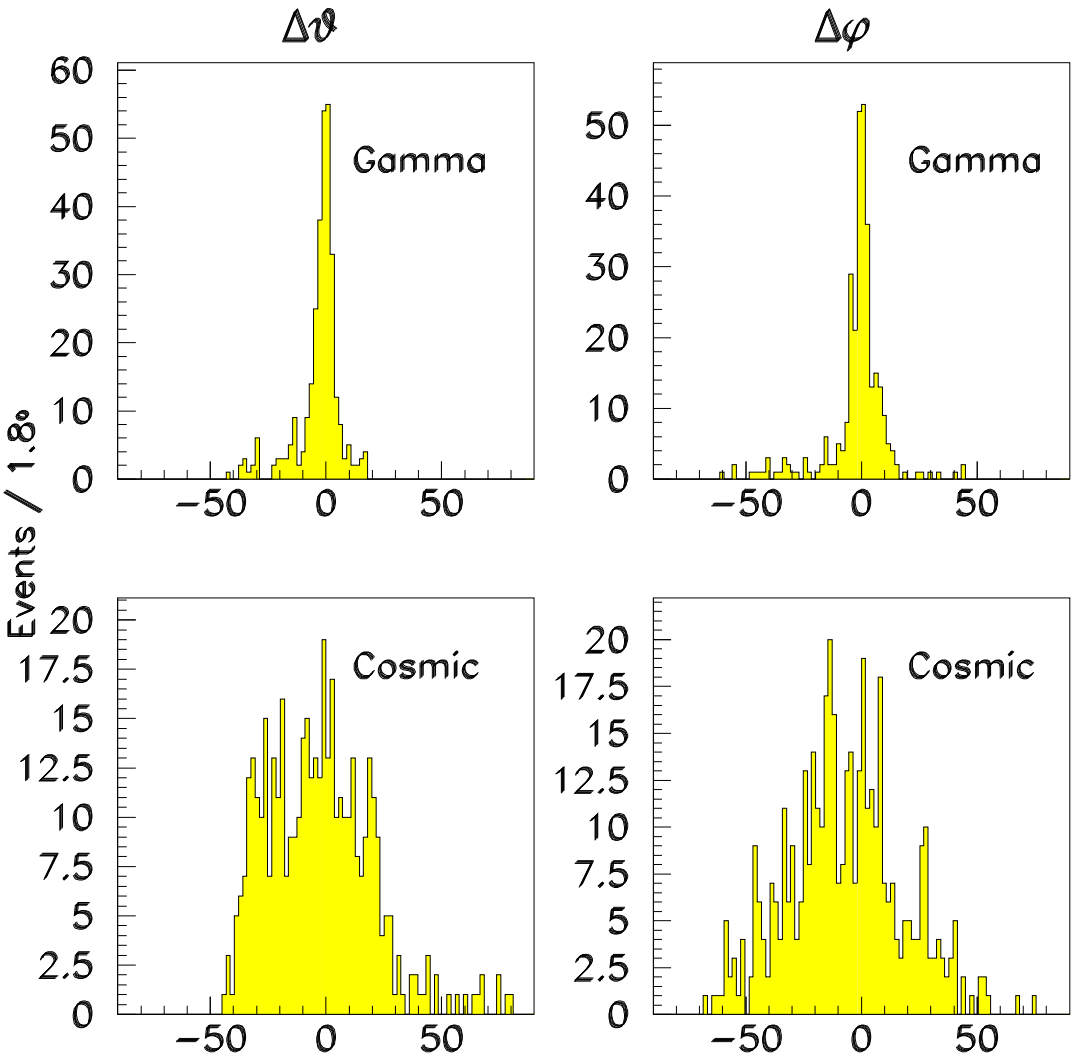

Figure 2: Distributions in the differences in polar and azimuthal angles (in degrees) between the shower axis and the line to the shower barycenter for single photon events and for events produced by cosmic rays as identified in the 2215-event scan.

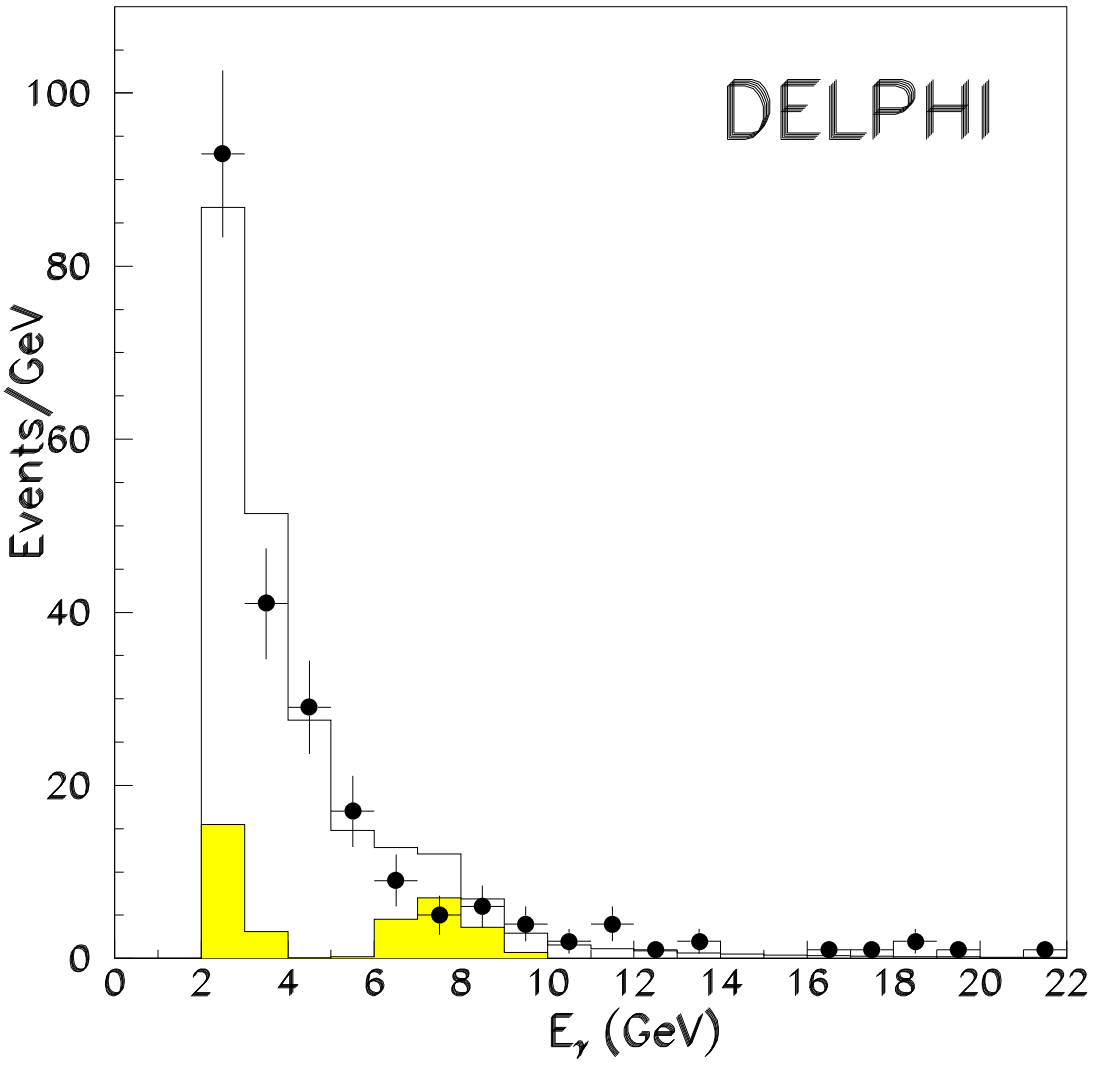

Figure 3: Distribution in energy of the single photon events (points). The histogram shows the expected distribution from the signal $\nu\bar{\nu}\gamma$ events plus the background $e^+e^-\gamma$ events (shaded region) in which the final state positron and electron escape detection.

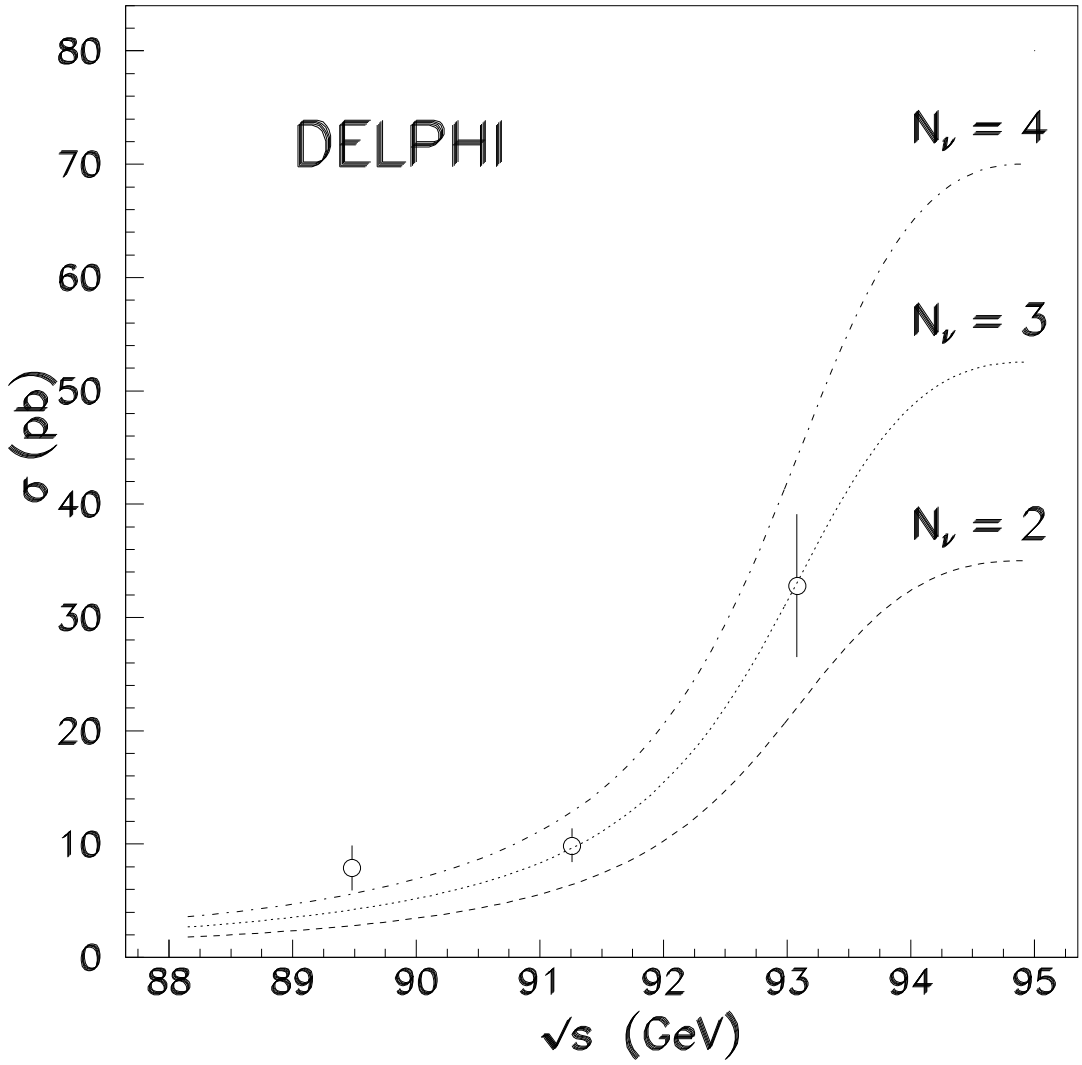

Figure 4: Measured cross sections for the reaction $e^+e^- \to \nu\bar{\nu}\gamma$ with $E_\gamma > 2$ GeV and $|\cos\vartheta_\gamma| < 0.7$, including all corrections and background subtractions. The curves show the expected distributions for two, three and four generations.

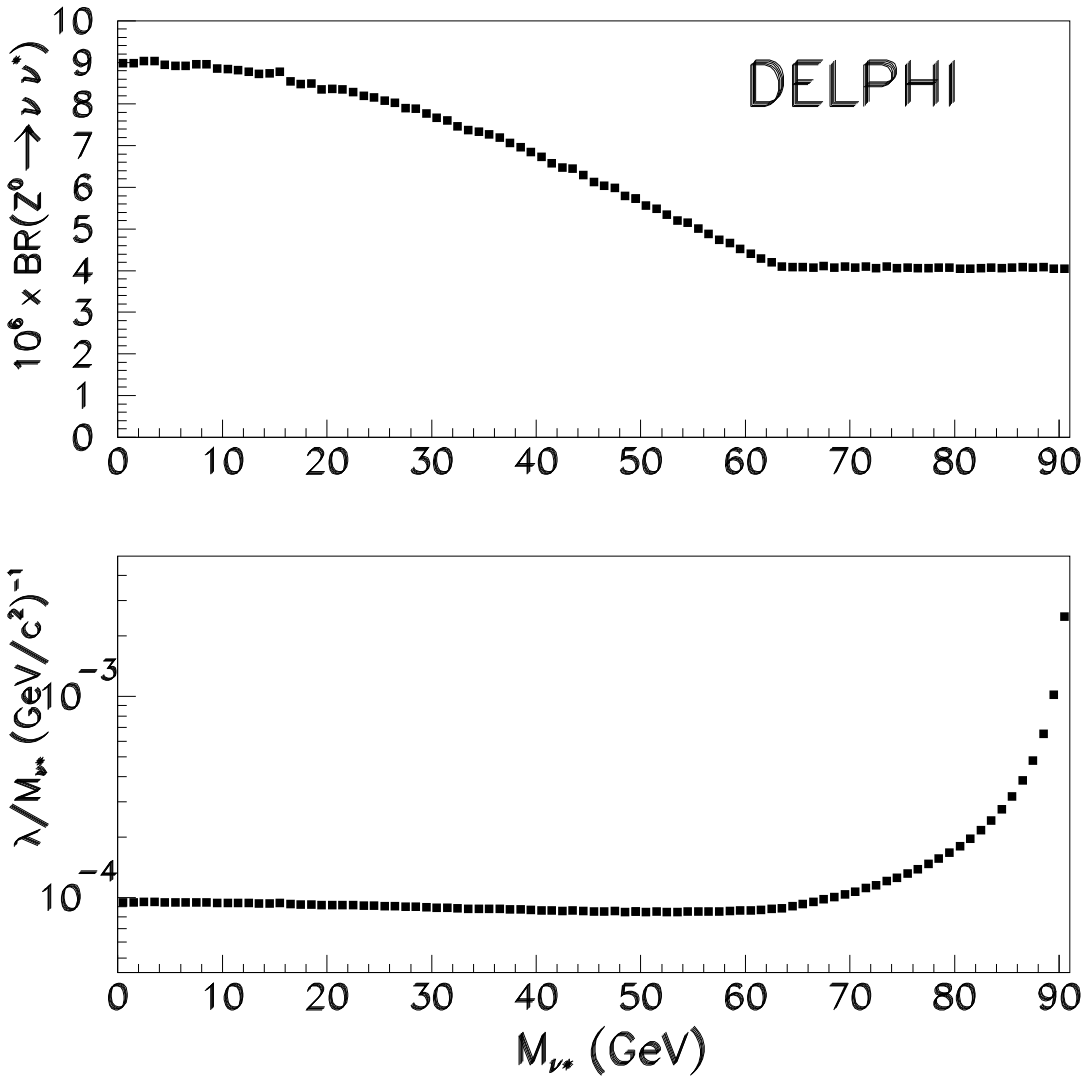

Figure 5: Limits at the 95% confidence level of BR($Z^0 \to \nu^*\bar{\nu}$) and λ/M_{ν^*} as functions of M_{ν^*}.

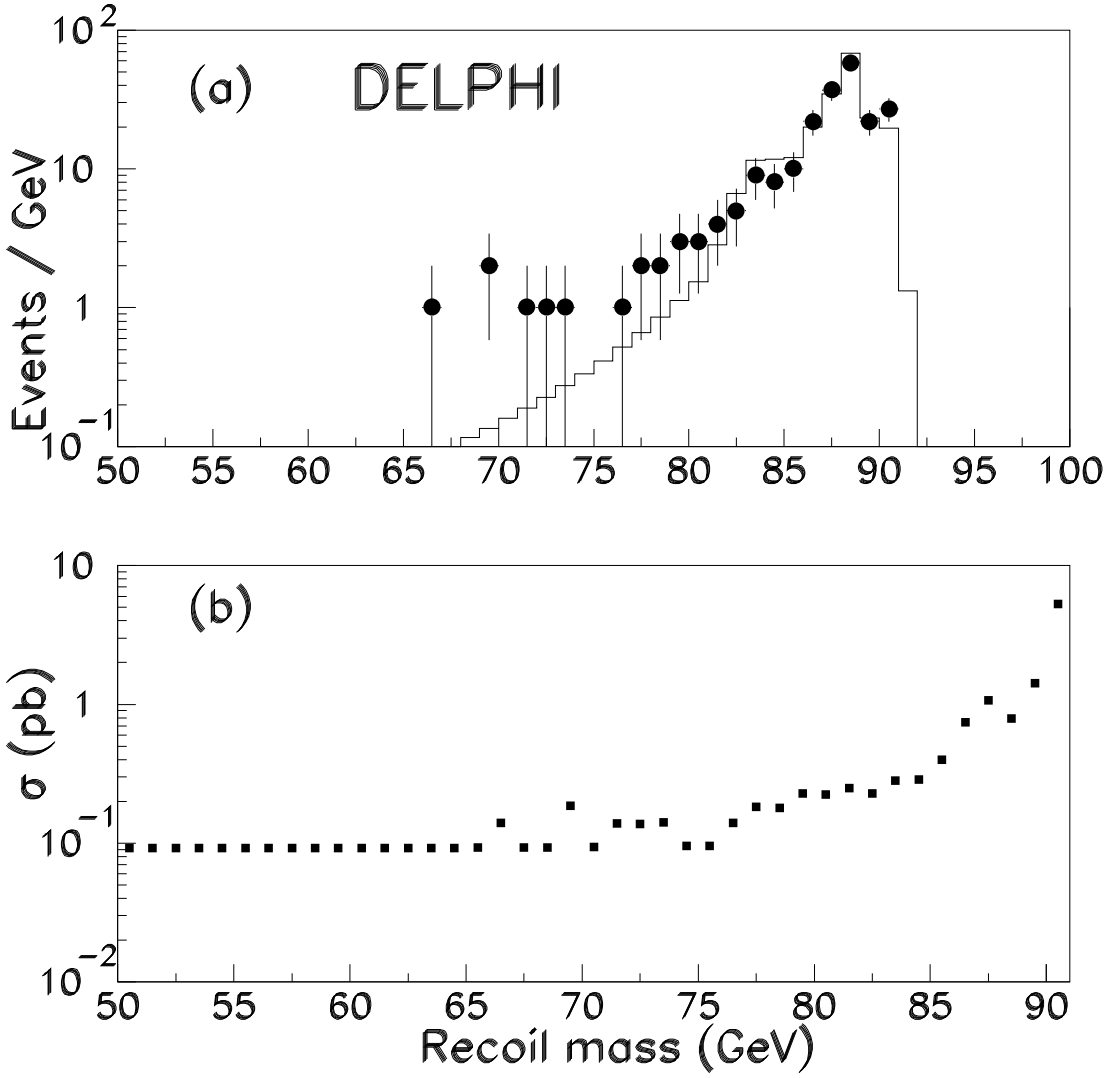

Figure 6: (a) Recoil mass distribution for the 219 single photon events (points) compared with the expectation for $\nu\bar{\nu}\gamma$ with $N_\nu = 3$ plus the known background processes (histogram). (b) Upper limit at the 95% confidence level for the production cross section of γ'X' with the photon in the range $|\cos\vartheta_\gamma| < 0.7$.